Journal of Alloys and Compounds 790 (2019) 524–528

Contents lists available at ScienceDirect

Journal of Alloys and Compounds

journal homepage: http://www.elsevier.com/locate/jalcom

In-situ synthesis of nanocrystalline soft magnetic Fe-Ni-Si-B alloy

J.G. Wang [a, b, *], H. Zhao [a], C.X. Xie [b], C.T. Chang [b, **], S.M. Zhou [b], J.Q. Feng [c], J.T. Huo [c], W.H. Li [a]

[a] School of Materials Science and Engineering, Anhui University of Technology, Ma'anshan 243002, China
[b] College of Mechanical Engineering, Dongguan University of Technology, Dongguan 523808, China
[c] Ningbo Institute of Materials Technology & Engineering, Chinese Academy of Sciences, Ningbo 315201, China

ARTICLE INFO

Article history:
Received 24 January 2019
Received in revised form
13 March 2019
Accepted 14 March 2019
Available online 16 March 2019

Keywords:
Fe-based ribbon
Nanocrystal
In-situ synthesis
Magnetic properties

ABSTRACT

Fe-based nanocrystalline ribbons (e.g. FINEMET) has been applied widely in electric industry due to its excellent soft magnetic properties. However, their preparation involves annealing at high temperature for the formation of α-Fe nanograins, which not only consumes additional energy but results in the embrittlement of the ribbon. In this work, the ductile nanocrystalline ribbons of Fe-Ni-Si-B with good soft magnetic properties have been in-situ prepared just using the melt-spinning method. The nanocrystals have a size less than 45 nm. After the stress relief annealing, the ductility is still available and the magnetic performance is improved. It's worth noting that the industrial grade rather than analytically pure raw materials are used in this work. Therefore, the results have profound implications for academic study and engineering application.

1. Introduction

In principle, magnetism mainly originates from the electrons in materials, so it is not strongly affected by the atomic structure [1,2]. The exchange interaction is supposed to take effect among the nearest-neighbors [2], which implies the ferromagnetism in the disordered materials. When the first Fe-based glass of $Fe_{80}P_{13}C_7$ (at. %) was prepared by Duwez and Lin using "piston and anvil" technique [3], its soft ferromagnetic feature was readily accepted in the community. More importantly, Fe-based metallic glasses (MGs) are utilized by far most commonly out of all the developed MGs due to the excellent soft magnetic properties and low cost [4]. The flexible Fe-based glassy ribbon can be easily wound as the iron cores of various transformers used in electric and electronic industries. Compared with the conventional silicon steel, the Fe-based glassy ribbon has a lower coercivity and a higher electric resistance which both can reduce the iron loss and therefore save energy [1,4]. As a representative, $Fe_{78}Si_9B_{13}$ (Metglas 2605 S-2) was found to perform better than the silicon steel [5]. Afterwards, the $Fe_{73.5}Si_{13.5}B_9Nb_3Cu_1$ (FINEMET) with an ultrafine grain structure was developed by Yoshizawa et al. [6]. FINEMET has a superior performance in the high frequency range [7], and therefore many studies have followed its scenario to achieve the nanocrystalline microstructure in Fe-based ribbon [8–17]. However, the nanocrystallization remains a key issue.

For FINEMET, the fully glassy $Fe_{73.5}Si_{13.5}B_9Nb_3Cu_1$ was firstly prepared, then it was annealed at an elevated temperature to precipitate the ultrafine grains of α-Fe(Si) [6]. In fact, the conventional annealing was also taken advantage to nano-crystallize the Fe-based glasses in other studies, though different annealing temperatures were adopted [8,9,11,15]. It is found that crystallization even often happens to the free surface of the as-spun Fe-based ribbons in previous literature [7,9,10]. This is due to the poor glass forming ability (GFA) of these Fe-based alloys. As a result, the costly raw materials with high purity were used in order to prepare the fully glassy ribbon as the precursor of the nanocrystallized ribbon. On the other hand, the annealing itself is quite energy- and time-consuming, and it usually causes the embrittlement of the ribbon and therefore worsens the manufacturability in subsequent procedures.

In this study, the nanocrystalline Fe-Ni-Si-B ribbons with good soft magnetic properties have been in-situ synthesized by single-roller melt spinning just in the air. With no any annealing, the crystalline grains of less than 45 nm in size develop just during

* Corresponding author. School of Materials Science and Engineering, Anhui University of Technology, Ma'anshan 243002, China.
** Corresponding author.
E-mail addresses: wangjg@dgut.edu.cn (J.G. Wang), changct@dgut.edu.cn (C.T. Chang).

https://doi.org/10.1016/j.jallcom.2019.03.226
0925-8388/

quenching process. The ribbon is very ductile and it can undergo a 180° bending without break. This ductility is still available even after the ribbon is subject to a stress relief annealing. The magnetic properties of the Fe-Ni-Si-B ribbon are investigated. According to the measured coercivity (H_c), the nanocrystalline Fe-Ni-Si-B alloy of ribbon is a typical soft magnetic material. Its saturation magnetization (M_s) is found higher than that of FINEMET. Besides, one must learn that the industrial grade raw materials with low purity are used in this work, and the alloy contains no rare element like Nb, which definitely reduces the price [10].

2. Experimental

At first, ingots with the nominal compositions of $Fe_{70+x}Ni_{12-x}B_{14}Si_4$ (x = 0, 2, 6 and 10) were prepared by arc melting industrial grade pure Fe (99.8%), Ni (99.9%) and Si (99.9%) and Fe-B (99.0%) under Ar atmosphere. Just in air, these master ingots were remelted by induction, then the melts were expelled onto a rotating copper wheel to prepare ribbons about 1.5 mm wide and 20 μm thick. The microstructure of as-spun ribbons was investigated by x-ray diffraction (XRD) and electron transmission microscope (TEM). Thermal properties of the as-spun ribbons were evaluated using differential scanning calorimetry (DSC) at a heating rate of 20 K/min, during which the Curie temperatures were also determined in virtue of thermal effect for the transition of ferromagnetism to paramagnetism. The magnetization behavior was measured using vibrating sample magnetometer (VSM) under a maximum applied field of 800 kA/m, and the coercivity was measured with a DC B-H loop tracer under a maximum applied field of 800 A/m.

3. Results

Fig. 1a shows the as-spun $Fe_{80}Ni_2B_{14}Si_4$ ribbon of 24 μm in thickness prepared with a wheel speed $v_w = 45$ m/s. It can be bent as a letter "M", and no break happens to the free surface or the wheel surface, which suggests that the ribbon is ductile enough. The ductility survives a stress relief annealing for 10 min at 375 °C. Similarly, this ductility is also found in $Fe_{70+x}Ni_{12-x}B_{14}Si_4$ (x = 0, 2 and 6). If v_w is increased to 55 m/s, the ribbons are about 19 μm thick and also very ductile.

The XRD patterns for free surface and wheel surface are shown in Fig. 1b and c, respectively. Sharp Bragg peaks corresponding to the crystalline phases are clearly visible, which indicates that crystallization occurs in both surfaces. α-Fe(Si) and Fe_2B are found in the free surface, whereas only α-Fe(Si) is identified in the wheel surface. As a matter of fact, the surface crystallization has been confirmed and studied by Wan et al. [7] and Fan and Shen [9]. They found that the crystallization only happened to the free surface and the wheel surface was fully glassy. This is due to the faster cooling rate for the wheel surface. Moreover, Wan et al. [7] proved that just 1 μm thick skin of the free surface was crystallized and the rest was not. In this work, the crystallization seems to take place throughout the ribbon according to Fig. 1b and c. Using Debye-Scherrer equation for Fig. 1b, the average grain size d_a was estimated, as listed in Table 1. Obviously, $d_a < 45$ nm holds true for all the alloys, which means the ribbons are nanocrystalline in microstructure.

To corroborate nanocrystalline microstructure directly, the ribbons have been examined by TEM. Fig. 2a shows a typical TEM image of the microstructure in the as-spun ribbon of $Fe_{80}Ni_2B_{14}Si_4$ ($v_w = 45$ m/s). One can see that the nanocrystals have developed in the glass matrix, which is also reflected by the combination of halo ring for the glass matrix and diffraction spots for the nanocrystals in the selected area electron diffraction (SAED) pattern (see the inset). Meanwhile, both lattice fringe of the nanocrystal and maze-like structure of the glass matrix are clearly shown by the high resolution TEM (HRTEM) in Fig. 2b. Obviously, the nanocrystallization occurs during the quenching when the ribbon is being prepared. On the other hand, most of the nanocrystalline grains are smaller than 50 nm in size, consistent with the

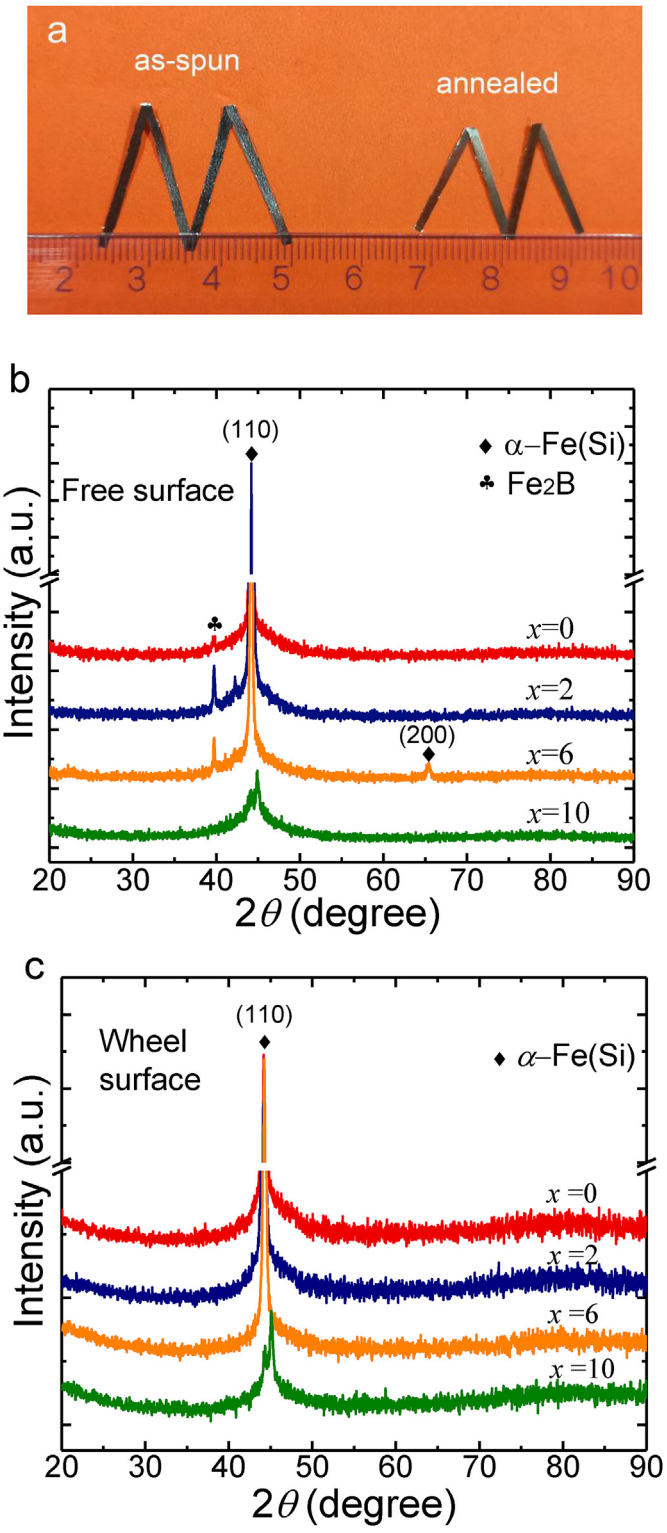

Fig. 1. (a) As a representative, the as-spun and annealed (375 °C, 10 min) ribbons of $Fe_{80}Ni_2B_{14}Si_4$ are bent as a letter "M", which indicates the good bending ductility. XRD patterns are presented for the free surface (b) and wheel surface (c) of all the as-spun ribbons of $Fe_{70+x}Ni_{12-x}B_{14}Si_4$ (x = 0, 2, 6 and 10).

Table 1
The characteristic data of as-spun nanocrystalline ribbons of $Fe_{70+x}Ni_{12-x}B_{14}Si_4$.

Alloy	d_a (nm)	T_c (°C)	T_x (°C)	M_s (emu/g)	H_c (A/m)
$x=0$	37	396	460	162.7	17.9
$x=4$	44	427	474	165.8	22.3
$x=8$	41	408	501	163.9	19.8
$x=10$	28	416	528	164.4	20.5
$x=10$[a]	–	401	493	161.5	27.2

[a] In comparison, the glassy ribbon prepared at $v_w = 55$ m/s is also measured.

estimation by XRD. They are almost equiaxed rather than dendritic. This morphology is very similar to that of FINEMET [6] or other Fe-based ribbons such as $Fe_{76.5}Cu_1Si_{13.5}B_9$ subject to annealing [18]. It demonstrates that the in-situ formation of nanocrystal is possible in Fe-based ribbons. In addition, it is found that the microstructure can be readily tailored or controlled by the wheel speed v_w, since the fully glassy nature of the ribbon with $v_w = 55$ m/s has been confirmed by TEM (see Fig. S1).

Fig. 3 presents two DSC curves for the as-spun $Fe_{80}Ni_2B_{14}Si_4$ ribbons prepared at $v_w = 45$ m/s (Fe80n) and $v_w = 55$ m/s (Fe80 g). One should learn that the ribbon for Fig. 3b is of full glass with no any crystalline phase (see Fig. S1). Like many other Fe-based glassy ribbons [19], the feature of glass transition is not clearly visible on the DSC curves in Fig. 3a and b. However, the transition of ferromagnetism to paramagnetism has been detected during the heating in DSC measurement, labelled as T_c (Curie temperature). $T_c = 416$ °C for Fe80n is obviously higher than $Tc = 401$ °C for Fe80 g. T_c for $Fe_{70+x}Ni_{12-x}B_{14}Si_4$ ($x = 0$, 2 and 6) nanocrystalline ribbons is also listed in Table 1. There seems no regularity for T_c vs. x to follow. Moreover, the exothermic events are distinctly found on the DSC curve, which indicates that the crystallization should happen to the glass matrix in the nanocrystalline ribbon [20]. The crystallization temperature T_x increases with the Ni content x, and it is higher than T_c (see Fig. 3 and Table 1). As expected, the crystallization occurs at a lower temperature in Fe80 g ($T_x = 493$ °C) than in Fe80n ($T_x = 528$ °C). This suggests that the nanocrystalline particles thermodynamically stabilize the matrix which is more resistant to the crystallization.

For estimation of the fraction of crystalline phase (P_c) in Fe80n, we calculate the crystallization enthalpy ΔH in both Fe80n and Fe80 g. As shown by the shade area in Fig. 3, ΔH_n for Fe80n is 60.3 J/g while ΔH_g for Fe80 g is 138.2 J/g. Therefore, it yields $P_c = \frac{\Delta H_g - \Delta H_n}{\Delta H_g} = 56.4\%$. This is basically consistent with the TEM observation (see Fig. 2a). On the other hand, as shown in Fig. 2a, the glass matrix, although taking up less volume fraction, is continuously connected, whereas the crystalline phase is isolated as islands. This may be the reason for bending ductility in the nanocrystalline ribbon (see Fig. 1a).

A higher T_c means that the ferromagnetism can keep at a higher temperature, which enables the magnetic materials to be used in a wider temperature range. In this sense, as presented in Fig. 3, Fe80n is undoubtedly preferable to Fe80 g. As well known, the saturation magnetization M_s is a more important parameter for the soft magnetic materials. Fig. 4a shows the relationship between the applied magnetic field H and the magnetization M, i.e. magnetization curve. The as-spun F80n ribbon (green curve) has a M_s of 164.4 emu/g under an applied magnetic field of 800 kA/m at room temperature. If the density of ingot $\rho = 7.58$ g/cm^3 is approximately taken as the density of the ribbon, the corresponding saturated magnetic polarization $J_s = 1.57$ T is calculated, remarkably higher than $J_s = 1.24$ T for FINEMET [6]. It is close to $J_s = 1.49$ T for the annealed $Fe_{80}P_{11}C_9$ [21] and $J_s = 1.56$ T of annealed Metglas 2605-S2 [22]. The annealing for Fe-based glass ribbons usually has a dual effect [6,18,22,23], i.e. precipitation of α-Fe nanocrystals and relief of residual stress. For Fe80n in this work, it is of course unnecessary to precipitate α-Fe nanograins via annealing around T_x, but the annealing for stress relief should be conducted due to the residual stress inside the ribbon caused by quenching. The annealing for stress relief is often performed at a temperature much lower than T_x. Therefore, Fe80n is annealed at 375 °C for 10 min, 153 °C lower than its T_x. Its magnetization behavior is presented by the red curve in Fig. 4a. In comparison, the annealed Fe80n has a higher M_s of 168.5 emu/g (J_s~1.61 T) than the as-spun counterpart, because the residual stress that impedes the motion of magnetic domain wall is partly removed [1]. For this reason, one can infer that the coercivity H_c in the annealed ribbon must decrease. This is proved in Fig. 4b. H_c is greatly reduced from 20.5 A/m for the as-spun Fe80n to 5.9 A/m for the annealed. In fact, the stress relief annealing was often conducted to lower H_c in many previous studies [22,24–26].

To optimize the annealing temperature, the Fe80n is also annealed for 10 min at 400 °C and 425 °C. In comparison, both M_s and H_c are almost the same for the ribbons annealed at 375 °C and 400 °C (see Fig. S2). However, when the annealing temperature is elevated to 425 °C, M_s decreases and H_c increases. In other words, the soft magnetic properties are deteriorated. Consequently, annealing at 375 °C is preferable in Fe80n. Similarly, many previous studies demonstrated that the stress relief annealing would be conducted below 400 °C in Fe-based ribbons [22,24,25].

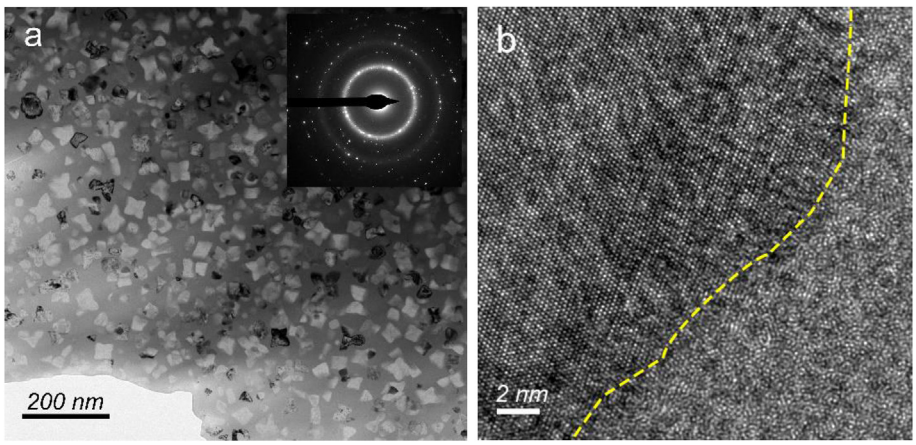

Fig. 2. The TEM investigation on the as-spun ribbon of $Fe_{80}Ni_2B_{14}Si_4$. (a) The nanocrystalline phase with a grain size of about 30 nm is surrounded by the glassy matrix, which basically agrees with the SAED pattern in the inset. (b) The HRTEM image of the crystalline phase and the glass separated by the dashed yellow line. (For interpretation of the references to colour in this figure legend, the reader is referred to the Web version of this article.)

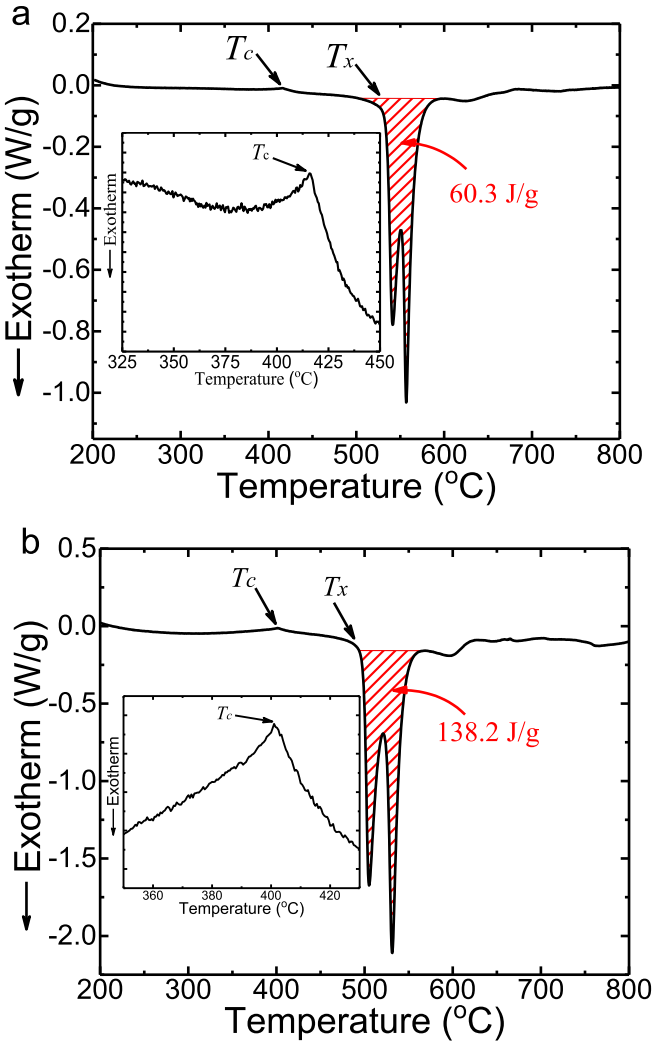

Fig. 3. The DSC curves for the as-spun nanocrystallized (a) and fully glassy (b) ribbons of $Fe_{80}Ni_2B_{14}Si_4$. According to the difference of crystallization enthalpy between them, the fraction of crystalline phase is estimated in the nanocrystalline ribbon. The curie temperature T_c (see the inset) and the crystallization temperature T_x are also determined.

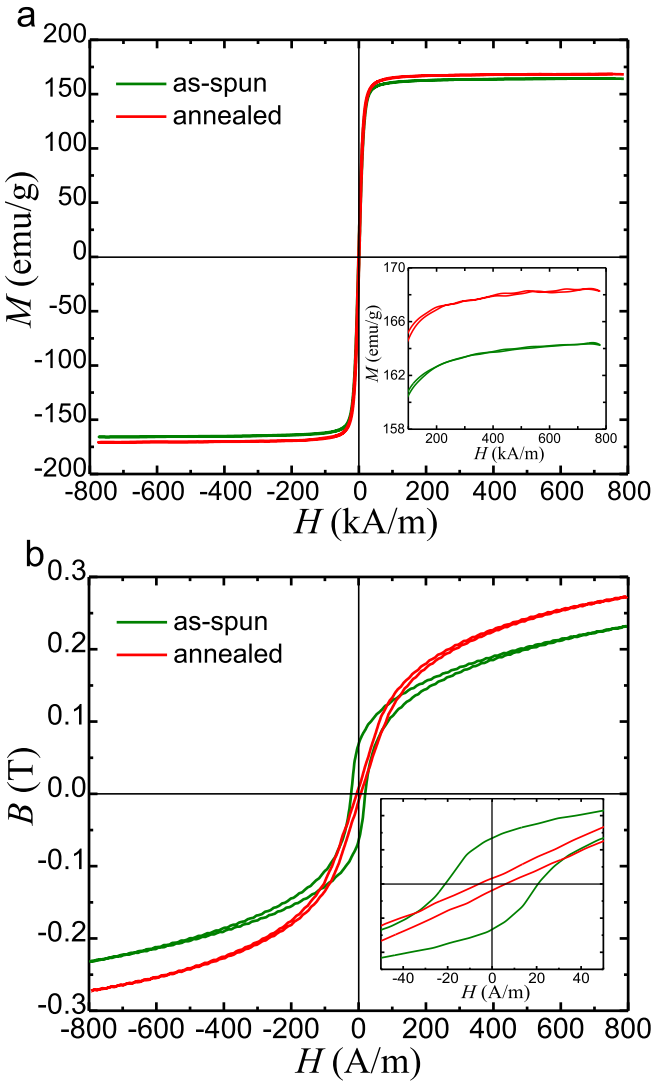

Fig. 4. (a) The magnetization curves and (b) the coercivity measurements for the as-spun (green) and annealed (red) nanocrystalline ribbons of $Fe_{80}Ni_2B_{14}Si_4$. Clearly, the ribbon annealed at 375 °C for 10 min has a higher M_s and a smaller H_c than the as-spun one. (For interpretation of the references to colour in this figure legend, the reader is referred to the Web version of this article.)

4. Discussion

The strategy for the preparation of FINEMET is not adopted in this work. Although Cu and Nb addition helps to form the ultrafine grains, it reduces M_s. Ni is ferromagnetic, and it is expected to confuse the system with little harm for the magnetic performance [27]. Raw materials of low purity are used in order that the impurities provide profuse nucleation sites to facilitate the formation of nanocrystals. Meanwhile, when wheel speed $v_w = 55$ m/s is applied, $Fe_{80}Ni_{12}B_{14}Si_4$ can be prepared as glass, and its glassy nature has been verified by TEM, SAED and HRTEM in Fig. S1. Its $M_s = 161.5$ emu/g ($J_s = 1.54$ T) and $H_c = 27.2$ A/m indicates that the glass is inferior to its nanocrystalline counterpart in terms of soft magnetic properties, which is presented in Fig. S3.

As listed in Table 1 and shown in Fig. 2a, the average grain size d_a in the ribbon of this work is several times larger than that of about 10 nm in FINEMET [6]. It is generally believed that 10–20 nm is good for the magnetic properties due to the small anisotropy resulting from the averaging effect among a number of neighboring grains and the lower magnetostriction [6,23]. Unfortunately, we find that it is difficult to control d_a in our present work, and d_a is usually larger than 20 nm once the crystalline phase develops. Furthermore, the α-Fe phase takes up no more than 56.4% in volume (see Fig. 3). There is also the Fe_2B phase in the ribbon (see Fig. 1a), and Fe_2B has a small M_s and a large H_c [28]. As a result, the soft magnetic performance is not so good as that of the new Fe-based nanocrystalline ribbons recently prepared in a manner for FINEMET [22,24,29,30]. However, the in-situ formation of nanocrystal during spinning-quenching helps the ribbon get rid of annealing at high temperature around T_x, and therefore the embrittlement is significantly alleviated and the ductility is kept even after the stress relief annealing (see Fig. 1a), which improves the damage tolerance of the material and the qualified rate of the product.

5. Conclusions

In summary, the nanocrystalline ribbons of $Fe_{70+x}Ni_{12-x}B_{14}Si_4$ (x = 0, 2, 6 and 10) with good soft magnetic properties have

successfully been synthesized using the simple method of melt-spinning. The nanocrystals are formed in-situ during the spinning process, which prevents the ribbons from the annealing at high temperature around T_x for the precipitation of α-Fe nanograins. Therefore, the bending ductility is kept after the ribbon is annealed for stress relief at a temperature much lower than T_x. As a representative, the nanocrystalline ribbon of $Fe_{80}Ni_{12}B_{14}Si_4$ has a higher Curie temperature and saturation magnetization, a smaller coercivity than its glass counterpart. Its magnetic properties can be improved further after the residual stress is substantially removed. More importantly, the raw materials with low purity are used and remarkably lower the cost of ribbon. This work may help produce nanocrystalline soft magnetic Fe-based ribbons in a simple and economical way and therefore expand their applications.

Acknowledgments

We gratefully appreciate the financial support by National Natural Science Foundation of China (Grant No. 51871056) and China Postdoctoral Science Foundation (Grant No. 2014M561550).

Appendix A. Supplementary data

Supplementary data to this article can be found online at https://doi.org/10.1016/j.jallcom.2019.03.226.

References

[1] B.D. Cullity, C.D. Graham, Introduction to Magnetic Materials, John Wiley & Sons, Inc., Hoboken, New Jersey, 2009.
[2] H.S. Chen, Glassy metals, Rep. Prog. Phys. 43 (1980) 353–432.
[3] P. Duwez, S.C.H. Lin, Amorphous ferromagnetic phase in iron-carbon-phosphorus alloys, J. Appl. Phys. 38 (1967) 4096–4097.
[4] C. Suryanarayana, A. Inoue, Bulk Metallic Glasses, Taylor & Francis Group, 2011.
[5] B.A. Luciano, C.S. Kiminami, An amorphous core transformer: design and experimental performance, Mater. Sci. Eng. A 226–228 (1997) 1079–1082.
[6] Y. Yoshizawa, S. Oguma, K. Yamauchi, New Fe-based soft magnetic alloys composed of ultrafine grain structure, J. Appl. Phys. 64 (1988) 6044–6046.
[7] F. Wan, T. Liu, F. Kong, A. Wang, M. Tian, J. Song, J. Zhang, C. Chang, X. Wang, Surface crystallization and magnetic properties of FeCuSiBNbMo melt-spun nanocrystalline alloys, Mater. Res. Bull. 96 (2017) 275–280.
[8] A. Urata, H. Matsumoto, S. Yoshida, A. Makino, Fe–B–P–Cu nanocrystalline soft magnetic alloys with high Bs, J. Alloys Compd. 509 (2011) S431–S433.
[9] X.D. Fan, B.L. Shen, Crystallization behavior and magnetic properties in High Fe content FeBCSiCu alloy system, J. Magn. Magn. Mater. 385 (2015) 277–281.
[10] L. Xie, T. Liu, A. He, Q. Li, Z. Gao, A. Wang, C. Chang, X. Wang, C.T. Liu, High Bs Fe-based nanocrystalline alloy with high impurity tolerance, J. Mater. Sci. 53 (2017) 1437–1446.
[11] N. Yodoshi, S. Ookawa, R. Yamada, N. Nomura, K. Kikuchi, A. Kawasaki, Effects of nanocrystallisation on saturation magnetisation of amorphous $Fe_{76}Si_9B_{10}P_5$, Mater. Res. Lett. 6 (2017) 100–105.
[12] Y. Jia, Z. Wang, F. Wang, L. Zhang, H. Duan, Effect of Ti on structure and soft magnetic properties of Si-rich Finemet-type nanocrystalline $Fe_{73.5}Cu_1Nb_{3-x}Si_{17.5}B_5Ti_x$ alloys, Mater. Res. Bull. 106 (2018) 296–300.
[13] M. Kuhnt, X. Xu, M. Amalraj, P. Kozikowski, K.G. Pradeep, T. Ohkubo, M. Marsilius, T. Strache, C. Polak, M. Ohnuma, K. Hono, G. Herzer, The effect of Co addition on magnetic and structural properties of nanocrystalline (Fe,Co)-Si-B-P-Cu alloys, J. Alloys Compd. 766 (2018) 686–693.
[14] K. Suzuki, R. Parsons, B. Zang, K. Onodera, H. Kishimoto, T. Shoji, A. Kato, Nano-crystallization of amorphous alloys by ultra-rapid annealing: an effective approach to magnetic softening, J. Alloys Compd. 735 (2018) 613–618.
[15] A. Martone, B. Dong, S. Lan, M.A. Willard, Iron-rich $(Fe_{1-x-y}Ni_xCo_y)_{88}Zr_7B_4Cu_1$ nanocrystalline magnetic materials for high temperature applications with minimal magnetostriction, AIP Adv. 8 (2018), 056126.
[16] Z. Lu, H. Li, Z. Lei, C. Chang, X. Wang, Z. Lu, The effects of metalloid elements on the nanocrystallization behavior and soft magnetic properties of FeCBSiPCu amorphous alloys, Metals 8 (2018) 283.
[17] Y.M. Chen, T. Ohkubo, M. Ohta, Y. Yoshizawa, K. Hono, Three-dimensional atom probe study of Fe–B-based nanocrystalline soft magnetic materials, Acta Mater. 57 (2009) 4463–4472.
[18] T. Kulik, Nanocrystallization of metallic glass, J. Non-Cryst. Solids 287 (2001) 145–161.
[19] M. Zhang, A. Wang, W. Yang, B. Shen, Effect of Fe to P concentration ratio on structures, crystallization behavior, and magnetic properties in $(Fe_{0.79+x}P_{0.1-x}C_{0.04}B_{0.04}Si_{0.03})_{99}Cu_1$ alloys, J. Appl. Phys. 113 (2013) 17A337.
[20] J.G. Wang, H. Yang, Y. Pan, Y.J. Song, W.H. Li, Y.Z. He, Structure transformation and fractography in $Zr_{20}Ti_{20}Cu_{20}Ni_{20}Be_{20}$ metallic glass, J. Non-Cryst. Solids 452 (2016) 273–279.
[21] J. Wang, R. Li, N. Hua, L. Huang, T. Zhang, Ternary Fe–P–C bulk metallic glass with good soft-magnetic and mechanical properties, Scripta Mater. 65 (2011) 536–539.
[22] A. Wang, C. Zhao, H. Men, A. He, C. Chang, X. Wang, R.-W. Li, Fe-based amorphous alloys for wide ribbon production with high B_s and outstanding amorphous forming ability, J. Alloys Compd. 630 (2015) 209–213.
[23] Z.H. Lai, H. Conrad, G.Q. Teng, Y.S. Chao, Nanocrystallization of amorphous Fe-Si-B alloys using high current density electropulsing, Mater. Sci. Eng. A 287 (2000) 238–247.
[24] C. Zhao, A. Wang, S. Yue, T. Liu, A. He, C. Chang, X. Wang, C.-T. Liu, Significant improvement of soft magnetic properties for Fe(Co)BPSiC amorphous alloys by magnetic field annealing, J. Alloys Compd. 742 (2018) 220–225.
[25] Y. Han, J. Ding, F.L. Kong, A. Inoue, S.L. Zhu, Z. Wang, E. Shalaan, F. Al-Marzouki, FeCo-based soft magnetic alloys with high B_s approaching 1.75 T and good bending ductility, J. Alloys Compd. 691 (2017) 364–368.
[26] Y. Han, F.L. Kong, F.F. Han, A. Inoue, S.L. Zhu, E. Shalaan, F. Al-Marzouki, New Fe-based soft magnetic amorphous alloys with high saturation magnetization and good corrosion resistance for dust core application, Intermetallics 76 (2016) 18–25.
[27] A.L. Greer, Metallic glasses, Science 267 (1995) 1947–1953.
[28] K.A. Murphy, N. Hershkowitz, Temperature-dependent hyperfine interactions in Fe_2B, Phys. Rev. B 7 (1973) 23–31.
[29] A. Wang, C. Zhao, A. He, H. Men, C. Chang, X. Wang, Composition design of high B_s Fe-based amorphous alloys with good amorphous-forming ability, J. Alloys Compd. 656 (2016) 729–734.
[30] Y.Q. Wu, T. Bitoh, K. Hono, A. Makino, A. Inoue, Microstructure and properties of nanocrystalline Fe–Zr–Nb–B soft magnetic alloys with low magnetostriction, Acta Mater. 49 (2001) 4069–4077.